Published in *Materials Science and Engineering A*, 626, 2015, pp9-15. doi:10.1016/j.matlet.2015.03.066

Structural impact on the Hall-Petch relationship in an Al-5Mg alloy processed by high-pressure torsion.

Piotr Bazarnik[a], Yi Huang[b], Malgorzata Lewandowska[a,*], Terence G. Langdon[b,c]

[a] Warsaw University of Technology, Faculty of Materials Science, Woloska 141, 02-507 Warsaw, Poland

[b] Materials Research Group, Faculty of Engineering and the Environment, University of Southampton, Southampton SO17 1BJ, UK

[c] Departments of Aerospace & Mechanical Engineering and Materials Science, University of Southern California, Los Angeles, CA 90089-1453, USA

Abstract

The evolution of microstructure and microhardness was studied in a commercial 5483 Al-5Mg alloy processed by high pressure torsion (HPT) under a pressure of 6.0 GPa up to 10 turns. Significant grain size refinement was observed even after 1/4 turn and additional processing led to a further grain size reduction and a shift in the distribution of grain boundary misorientation angles towards higher values. An essentially fully homogeneous microstructure was reached after 10 turns with a final grain size of ~70 nm, a saturation Vickers microhardness of Hv ≈ 240 which was attained at and above equivalent strains of ~150, a relatively narrow grain size distribution and a fraction of ~80% of high-angle grain boundaries. Analysis shows the Hall-Petch plot deviates from the conventional linear relationship for samples processed through small numbers of turns but after 3 or more turns there is a direct correlation between the results obtained in HPT processing and coarse-grained samples.

Keywords: Al-Mg alloy; Hall-Petch relationship; high-pressure torsion; microhardness; ultrafine grains

[*]Corresponding author: Malgorzata Lewandowska (malew@inmat.pw.edu.pl)

1. Introduction

It is well known that grain refinement leads to a significant increase in strength in metals due to the Hall-Petch relationship [1,2] which correlates the mechanical properties with microstructural features such as the grain size. This relationship demonstrates the potential for improving the mechanical strength by reducing the grain size and this has been a major driving force in the development of ultrafine grained (UFG) and nanocrystalline (NC) materials. In practice, these materials are most readily produced in bulk form by subjecting materials to severe plastic deformation (SPD).

A number of techniques are now available for the SPD processing of metals [3-6] but the procedures receiving the most attention are equal-channel angular pressing (ECAP) [7] and high-pressure torsion (HPT) [8]. Both of these methods impose high strains but in practice the largest strains are imposed by HPT and, by comparison with other available SPD procedures, HPT processing gives the smallest grains [9,10] and the highest fraction of high-angle grain boundaries [11].

During HPT processing, a thin disk is placed horizontally between two massive anvils, it is subjected to a high pressure and then strained torsionally through rotation of one of the anvils. In order to compare the shear strain in HPT with linear strain values for other SPD methods, the equivalent von Mises strain, ε_{eq}, is expressed for HPT as [12]

$$\varepsilon_{eq} = \frac{2\pi N r}{h\sqrt{3}} \qquad (1)$$

where N is the number of turns, r is the distance from the centre of the disk and h is the sample thickness. It follows from eq. (1) that the strain varies across the disk and reaches zero at the disk centre where $r = 0$. This suggests that the microhardness distributions will be extremely inhomogeneous but numerous reports show there is usually a gradual evolution

with increasing strain towards a reasonable level of structural homogeneity [13-19]. Furthermore, this evolution is consistent with theoretical modelling [20].

Only limited information is currently available on the microstructure and mechanical properties of 5XXX series aluminium alloys processed by HPT. There are also shortcomings in the data because the disks are often processed up to only 5 turns of HPT [21,22] which may be insufficient to attain a high level of homogeneity and there has been no attempt to evaluate the significance of the grain boundary (GB) characteristics, and especially the boundary misorientations, in determining the properties of the alloy. In practice, the GB characteristics are important in metals processed by SPD because the misorientation angles change significantly during processing such that many of the low-angle grain boundaries (LAGBs) evolve into high-angle grain boundaries (HAGBs). There have been some discussions on the influence of the GB misorientation distributions on the mechanical properties [23,24] but there are only limited experimental results to address this problem [25-27]. Accordingly, the present research was initiated to evaluate the influence of HPT processing on the grain refinement, grain boundary characteristics and the homogeneity of a commercial AA5483 aluminium alloy processed by HPT.

2. Experimental material and procedures

The material investigated in this study was a hot-pressed commercial AA5483 aluminium alloy containing 5% Mg and 1% Mn with an average grain size of ~25 μm. The material was cut into disks with diameters of 10 mm and thicknesses of ~0.8 mm. These disks were polished and then processed at room temperature using quasi-constrained HPT [28,29] with a constant pressure of 6.0 GPa and a rotation speed of 1 rpm. Disks were torsionally strained through different numbers of revolutions, N, up to a maximum of 10.

After HPT processing, microhardness measurements were conducted on the polished surfaces of disks using an FM-300 microhardness tester. These measurements were taken

under a load of 100 g and a dwell time of 10 s. The values of the Vickers microhardness, Hv, were recorded for each disk both along a diameter with a separation between points of 0.3 mm and over the total areas of selected disks following a rectilinear grid with a spacing of 0.3 mm between each consecutive point.

For inspection using transmission electron microscopy (TEM), small disks with a diameter of 3 mm were punched from the edge regions of each disk so that the areas of observation were ~3.5 mm from the central points. This is shown in Fig. 1 where the illustration on the right depicts three different orientations for the TEM disks: orientation 1 is parallel to the HPT disk plane and orientations 2 and 3 are on the cross-sectional planes and either parallel or perpendicular to the rotation direction, respectively. These disks were cut using a focus ion beam microscope Hitachi FB 2100 and then experimental data were collected using an Hitachi 5500 STEM operating at an accelerating voltage of 30 kV. The microstructures were evaluated quantitatively using a computer-aided image analyzer. The grain sizes were described in terms of the equivalent grain diameter, d_{eq}, defined as the diameter of a circle with a surface area equal to the surface area of the grain. For the cross-sectional planes, the short and long axes of elongated grains were also measured. The standard deviations (SD) were estimated for all grain populations.

The GB misorientations were determined for samples cut parallel to the disk plane in orientation 1 using TEM with the Kikuchi patterns obtained for adjacent grains using convergent beam electron diffraction (CBED) [30]. Diffraction images were taken from neighbouring grains with a high resolution scanning TEM (Hitachi HD 2700) and then processed using a KILIN program to calculate the crystallographic orientations of individual grains and the misorientations across the GBs.

3. Experimental results

3.1 Evolution of microstructure during HPT

A series of representative TEM images are recorded in Fig. 2 for three disk planes after processing through (from the top row) 1/2, 1, 5 and 10 turns: the images in (a-d) show the structures visible on the disk plane (plane 1), (e-h) show the cross-sectional plane parallel to the rotation direction (plane 2) and (i-l) show the cross-sectional plane perpendicular to the rotation direction (plane 3). On plane 1, grain size quantification showed the average grain size was reduced to ~175 and ~155 nm after 1/4 and 1/2 turn, respectively. Further straining led to additional grain refinement and the detailed results and SD values are summarized in Table 1. After 10 revolutions the grain size was measured as ~70 nm which is significantly smaller than the size of ~100 nm recorded for the same alloy after processing by ECAP followed by hydrostatic extrusion [27] or ~200 nm recorded for the same alloy after processing after processing by hydrostatic extrusion [31].

Images taken from the two cross-sectional planes provide information on the three-dimensional size and shape of the grains formed during HPT processing. On plane 2 the grains are highly elongated with respect to the shearing direction and lie at angles between 45° and 55° to the disk plane. Measurements showed the shortest axes decreased with increasing N from ~100 nm for 1/2 turn to ~40 nm after 10 turns. A similar tendency was found on plane 3 as summarized in Table 2 but for this plane the grains were elongated along the disk diameter and the elongation was parallel to the surface.

Careful examination showed there were also differences in the grain size distributions. Processing with only 1/2 turn of HPT produced a highly inhomogeneous structure (Fig. 2a) with relatively large grains having diameters of ~1 μm surrounded by smaller grains with diameters from 100 to 200 nm. With increasing N, it is apparent that the grain structure gradually becomes more homogenous.

The distributions of GB misorientations angles are shown in Fig. 3 for samples processed through 1/2, 1, 5 and 10 turns with at least 100 boundaries examined in each sample. In general, the number fractions of LAGBs decrease and the number fractions of HAGBs increase with increasing *N*. The shapes of these distribution diagrams are typical for materials processed by SPD and in the present investigation the fraction of HAGBs reached a maximum of 80% after 10 turns.

3.2 Microhardness evolution across the disk diameters after HPT

The microhardness distributions across the disk diameters are shown in Fig. 4 for samples processed by HPT through different numbers of revolutions from 1/4 to 10. The lower dashed line at Hv ≈ 92 denotes the initial microhardness prior to processing. Inspection shows the microhardness increases significantly as a function of distance from the disk centre even after 1/4 turn. For this early condition, there is a clear linear dependence in the hardness values along the radius of the disk and this corresponds directly to the linear dependence of the applied strain in eq. (1). After 1/4 and 1/2 turn, the areas around the centres of the disks exhibit very low microhardness values with Hv ≈ 96 which is close to the value for the unprocessed sample whereas, by contrast, the hardness is Hv ≈ 160-180 near the edges of each disk. Nevertheless, after larger numbers of turns the central region undergoes significant strengthening and finally, after 10 turns, there is a reasonable level of homogeneity throughout the disk with a hardness of Hv ≈ 240.

3.3 Microhardness distributions over the total disk surfaces after HPT

Microhardness values were recorded following a grid pattern over the total surface of selected disks and the results are plotted as color-coded contour maps in Fig. 5. For all plots, the individual values of Hv are represented by a set of unique colours which defines incremental values of Hv in steps of 10 for hardness values in the range from 90 to 240. A similar procedure was introduced earlier for displaying hardness variations after HPT [13].

These contour maps depict the microhardness distributions over the entire surfaces of disks processed by HPT through various number of turns. It is readily apparent from Fig. 5 that all maps have radial symmetry which confirms that readings recorded along a single randomly selected diameter, as in Fig, 4, are valid for any diameter within the disk. The maps also consistently exhibit lower values of microhardness at the disk centres and higher values at the edges. The diameters of the central regions with lower hardness decrease markedly with increasing numbers of revolutions. In general, the samples exhibit a clear trend towards higher values of hardness and an increased hardness homogeneity with increasing *N*.

4. Discussion

4.1 Influence of applied strain on the microstructure and disk homogeneity

The present results provide unambiguous evidence that reasonably homogenous disks of the commercial AA5483 aluminium alloy may be obtained through HPT processing provided the straining is continued through a sufficient number of turns. This evolution is clearly visible in the microhardness diagram in Fig. 4 and the color-coded maps in Fig. 5. Nevertheless, there is a considerable hardness inhomogeneity after low numbers of turns and this is generally consistent with eq. (1). The gradual evolution to a high level of homogeneity has been reported for numerous materials [15,18,32-36] although recent results documented an inability to achieve homogeneity in the NiTi shape memory alloy even after processing through 40 turns [37].

It is instructive to note that the HPT processing of the Al-5483 alloy produced a UFG structure even in the initial stages of torsional straining. Thus, processing by only 1/4 turn produced an average grain size of ~175 nm. However, there was a considerable inhomogeneity in the grain size distribution after 1/4 turn with a large scatter in the grain size distribution. By contrast, after 10 turns the average grain size was reduced to ~70 nm and there was only a relatively small scatter in the grain size distribution. This level of grain

refinement is exceptionally large by comparison with other aluminium alloys processed by HPT. For example, the average grain sizes were ~500 nm in the AA7075 alloy after 10 revolutions [17], ~250 nm in AA6061 after 10 revolutions [14] and ~230 nm in an Al-1% Mg alloy after 10 revolutions [19].

There are also significant changes in the GB character distributions with increasing HPT turns. In the samples processed through small numbers of turns the distributions of GB misorientation angles is relatively wide with a high fraction of LAGBs of >40%. With increasing numbers of turns, there is a gradual increase in the misorientation angles and an evolution into HAGBs. Thus, after 10 turns approximately 80% of GBs have high angles of misorientation.

4.2 Hardness evolution as a function of applied strain

It was noted in an early report that hardness data of the type shown in Fig. 4 may be successfully correlated by plotting all of the datum points in the form of Hv against the equivalent strain [38]. This approach has been used for a large number of different metals [39-45] and a comprehensive review of the available data is now available [46]. Figure 6 shows a plot of Hv against equivalent strain where the strain was estimated using eq. (1). Thus, all of the datum points scatter about a curve but there is a general levelling of the results and a reasonable saturation condition is attained after an equivalent strain of ~150.

It was shown in the review on hardness distributions after HPT that the microhardness is generally consistent with one of three possible models: (i) there may be strain hardening with an ultimate saturation and no evidence for any recovery, (ii) there may be strain hardening with recovery and then a saturation or (iii) there may be a strain weakening [46]. The results in Fig. 6 follow the first model with rapid strain hardening up to a strain of ~20, moderate strain hardening thereafter and then saturation above a strain level of ~150. The strain of ~150 which is required to attain saturation is higher than in some other similar

aluminium-based alloys. For example, the saturation strain was ~30 in an Al-1% Mg solid solution alloy [19] and ~50 in an Al-0.6% Mg-0.4% Si alloy [33]. However, the material used in the present investigation contained 5% of Mg and therefore recovery was more difficult compared to these other materials where there was a much lower content of alloying elements. Therefore, it is reasonable to anticipate that the saturation condition will be reached at a significantly higher strain as shown by the maximum strain of ~200 recorded at the edge of the sample deformed through 10 turns. A lack of saturation for strains lower than ~150 in the present alloy is consistent with the microstructural observations where continuous grain refinement was observed with increasing numbers of turns as shown in Fig. 2. It is also consistent with earlier experimental data on an Al-6061 alloy processed by HPT [47].

4.3 The significance of GB characteristics in tailoring mechanical strength

The present results in Fig. 2 and Tables 1 and 2 show that HPT processing leads to a pronounced microstructural refinement in the 5483 aluminium alloy and therefore it is important to evaluate the significance of the GB characteristics.

The influence of grain size on the mechanical properties is usually written in the form of the Hall-Petch relationship either for the yield flow stress or for hardness. Thus,

$$\sigma = \sigma_o + k_y d^{-1/2} \quad (2)$$

where σ is the flow stress at a given plastic strain, σ_o and k_y are material constants and d is the average grain size or

$$H = H_o + k_H d^{-1/2} \quad (3)$$

where H is the hardness and H_o and k_H are material constants.

Both of these relationships have been confirmed for numerous materials [5,48-54] covering a wide range of grain sizes varying from hundreds of micrometers to dozens of nanometers. However, for very small grain sizes there are reports of a deviation from the typical Hall-Petch relationship and several recent reports have examined the significance of

the Hall-Petch relationship for these ultrafine grains [55-57]. For example, there is evidence for an inverse Hall-Petch effect at very small grain sizes, typically below ~25 nm [58], but there are also experimental results showing both essentially an independence of grain size at small grain sizes [33] and a significant increase in slope when the grain size is very small [59]. The reasons for these variations are not yet understood but it seems likely that differences in the GB characteristics play an important role.

In order to check the applicability of the Hall-Petch relationship for the 5483 aluminium alloy processed by HPT, the microhardness values obtained at the edges of the disks were plotted as a function of $d^{-1/2}$ together with datum points obtained for the same alloy with larger coarse grain sizes. The coarse-grained samples were obtained by annealing of the initial sample at 573 K for one hour and at 673 K for one and five hours. The result is shown in Fig. 7 where it is apparent that there is a conventional linear correlation between the data for the coarse-grained samples and for the samples processed by HPT through 3 or more turns whereas the values of microhardness for samples after 1/4, 1/2 and 1 turn lie below the line. This is consistent with Fig. 4 and the evolution into a reasonable level of homogeneity with additional torsional straining. From the slope of the experimental line in Fig. 7, the value of k_H is estimated as ~1430 Hv $nm^{1/2}$.

The deviation from the Hall-Petch relationship after low numbers of turns is due to the nature of the microstructure after fractional or small numbers of torsional revolutions. Thus, the Hall-Petch analysis considers only the average grain size but after small numbers of turns there are significant variations both in the distributions of the individual grain sizes and in the GB character distributions as demonstrated by measurements of the misorientation angles in Fig. 3. The significance of GB character distribution in tailoring the mechanical strength of metals was noted earlier for conventional coarse-grained materials where it was shown for an austenitic stainless steel that a higher fraction of special GBs led to a weaker strengthening

effect [60]. For SPD processed materials, the GBs differ in their misorientation angles as a direct consequence of the microstructural evolution during processing. Thus, as the applied strain increases, the distribution in the misorientation angles is shifted to higher values so that the fractions of HAGBs increases from about 55% to 80% when increasing the torsional straining from 1/2 to 10 turns, respectively.

It is well established that slip transfer through LAGBs is much easier by comparison with HAGBs and therefore they represent weaker barriers for the movement of lattice dislocations. The present results are consistent with a phenomenological model proposed earlier in which the HAGBs are strengthening elements within the microstructure whereas the LAGBs make only a minor contribution to the strength of the material [24]. This effect may be correlated with a model in which the stress is enhanced at HAGBs due to the formation of dislocation pile-ups and yielding then takes place when the stress is sufficiently large to initiate slip from one grain to the next. In this model, the LAGBs are then less effective in impeding dislocation slip due to the relatively smaller crystallographic misalignment across the grain boundaries.

5. Summary and conclusions

1. A commercial 5483 Al-5Mg alloy was processed by high-pressure torsion for various amounts of torsional straining between 1/4 and 10 turns.

2. The results show the microstructure evolves with torsional straining so that there is a continuous reduction in the average grain size, an increase in the average boundary misorientation angle and a corresponding narrowing in the grain size distribution.

3. After 10 turns, the average grain size was ~70 nm, the fraction of high-angle grain boundaries was about 80% and the microhardness was reasonably homogeneous across the disk with a saturation Vickers microhardness of Hv ≈ 240 that was attained at equivalent strains at and above ~150.

4. The results show the Hall-Petch plot provides a direct linear correlation between samples processed through 3 and more turns of HPT and data obtained on coarse-grained samples. There is a breakdown in this correlation for samples processed by HPT through only 1/4 to 1 turn because of the larger fractions of grain boundaries having low angles of misorientation.

Acknowledgements

This work was supported by the European Union in the framework of the European Social Fund through the Warsaw University of Technology Development Programme, realized by the Center for Advanced Studies. This research was financed by the National Centre for Research and Development within the project "New materials and technologies for lightweight generic components of electric low-emission concept vehicle" and it was also supported by the European Research Council under ERC Grant Agreement No. 267464-SPDMETALS.

References

[1] E.O. Hall, Proc. Phys. Soc. B, 64 (1951); pp. 747-753.

[2] N.J. Petch, J Iron Steel Inst., 174 (1953); pp. 25-28.

[3] R.Z. Valiev, R.K. Islamgaliev, I.V. Alexandrov, Prog. Mater. Sci., 45 (2000); pp. 103-189.

[4] R.Z. Valiev, Y. Estrin, Z. Horita, T.G. Langdon, M.J. Zehetbauer, Y.T. Zhu, JOM 58 (4) (2006); pp.33-39.

[5] I. Sabirov, M.Yu Murashkin, R.Z. Valiev, Mater. Sci. Eng. A, 560 (2013); pp. 1-24.

[6] T.G. Langdon, Acta Mater., 61 (2013); pp. 7035-7059.

[7] R.Z. Valiev, T.G. Langdon, Prog. Mater. Sci., 51 (2006); pp. 881-981.

[8] A.P. Zhilyaev, T.G. Langdon, Prog. Mater. Sci. 53 (2008); pp. 893-979.

[9] A.P. Zhilyaev, S. Lee, G.V. Nurislamova, R.Z. Valiev, T.G. Langdon, Scripta Mater., 44 (2001); pp. 2753-2758.

[10] A.P. Zhilyaev, G.C. Nurislamova, B.K. Kim, M.D. Baró, J.A. Szpunar, T.G. Langdon , Acta Mater., 51 (2003); pp. 753-765.

[11] J. Wongsa-Ngam, M. Kawasaki, T.G. Langdon, J. Mater. Sci., 48 (2013); pp. 4653-4660.

[12] R.Z. Valiev, Y.V. Ivanisenko, E.F. Rauch, B. Baudelet, Acta Mater., 44 (1996); pp. 4705-4712.

[13] C. Xu, Z. Horita, T.G. Langdon, Acta Mater., 55 (2007); pp. 203-212.

[14] C. Xu, Z. Horita, T.G. Langdon, Acta Mater., 56 (2008); pp. 5168-5176.

[15] M. Kawasaki, S.N. Alhajeri, C. Xu, T.G. Langdon, Mater. Sci. Eng. A, 529 (2011); pp. 345-351.

[16] M. Das, G. Das, M. Ghosh, M. Wegner, V. Rajnikan, S. GhoshChowdhury, T.K. Pal, Mater. Sci. Eng. A, 558 (2012); pp. 525-532.

[17] S. Sabbaghianrad, M. Kawasaki, T.G. Langdon, J. Mater. Sci., 47 (2012); pp. 7789-7795.

[18] M. Kawasaki, J. Foissey, T.G. Langdon, Mater. Sci. Eng. A, 561 (2013); pp. 118-125.

[19] O. Andreau, J. Gubicza, N.X. Zhang, Y. Huang, P. Jenei, T.G. Langdon, Mater. Sci. Eng. A, 615 (2014); pp. 231-239.

[20] Y. Estrin, A. Molotnikov, C.H.J. Davies, R. Lapovok, J. Mech. Phys. Solids., 56 (2008); pp. 1186-1202.

[21] Z. Lee, F. Zhou, R.Z. Valiev, E.J. Lavernia, S.R. Nutt, Scripta Mater., 51 (2004); pp. 209-214.

[22] A.A. Mazilkin, B.B. Straumal, E. Rabkin, B. Baretzky, S. Enders, S.G. Protasova, O.A. Kogtenkova, R.Z. Valiev, Acta Mater., 54 (2006); pp. 3933-3939.

[23] M. Furukawa, Z. Horita, M. Nemoto, R.Z. Valiev, T.G. Langdon, Acta Mater., 44 (1996); pp. 4619-4629.

[24] N. Hansen, Scripta Mater., 51 (2004); pp. 801-806.

[25] D.A. Hughes, N. Hansen, Acta Mater., 48 (2000); pp. 2985-3004.

[26] Q. Liu, X. Huang, D.J. Lloyd, N. Hansen, Acta Mater., 50 (2002); pp. 3789-3802.

[27] P. Bazarnik, B. Romelczyk, M. Kulczyk, M. Lewandowska, Mater. Sci. Forum, 765 (2013); pp. 423-428.

[28] R.B. Figueiredo, P.R. Cetlin, T.G. Langdon, Mater. Sci. Eng. A, 528 (2011); pp. 8198-8204.

[29] R.B. Figueiredo, P.H.R. Pereira, M.T.P. Aguilar, P.R. Cetlin, T.G. Langdon, Acta Mater., 60 (2012); pp. 3190-3198.

[30] R.M.J Bokel, F.W. Schapink,F.D. Tichelaar, Ultramicros., 75 (1998); pp. 183-195.

[31] J. Zdunek, P. Widlicki, H. Garbacz, J. Mizera, K.J. Kurzydłowski Solid State Phenom. 114 (2006) p. 171–176

[32] M. Kawasaki, B. Ahn, T.G. Langdon, Acta Mater., 58 (2010); pp. 919-930.

[33] A. Loucif, R.B. Figueiredo, T. Baudin, F. Brisset, R. Chemam, T.G. Langdon, Mater. Sci. Eng. A, 532 (2012); pp. 139-145.

[34] S. Sabbaghianrad, M. Kawasaki, T.G. Langdon, J. Mater. Sci., 47 (2012); pp. 7789-7795.

[35] A.Y. Khereddine, F.H. Larbi, M. Kawasaki, T. Baudin, D. Bradai, T.G. Langdon, Mater. Sci. Eng. A, 576 (2013); pp. 149-155.

[36] M. Shirooyeh, J. Xu, T.G. Langdon, Mater. Sci. Eng. A, 614 (2014); pp. 223-231.

[37] H. Shahmir, M. Nili-Ahmadabadi, Y. Huang, T.G. Langdon, J. Mater. Sci., 49 (2014); pp. 2998-3009.

[38] A. Vorhauer, R. Pippan, Scripta Mater., 51 (2001); pp. 921-925.

[39] K. Edalati, T. Fujioka, Z. Horita, Mater. Sci. Eng. A, 497 (2008); pp. 168-173.

[40] Y. Harai, K. Edalati, Z. Horita, T.G. Langdon, Acta Mater., 57 (2009); pp. 1147-1153.

[41] K. Edalati, Y. Ito, K. Suehiro, Z. Horita, Int. J. Mater. Res., 100 (2009); pp. 1668-1673.

[42] K. Edalati, T. Fujioka, Z. Horita, Mater. Trans., 50 (2009); pp. 44-50.

[43] K. Edalati, Z. Horita, Mater. Trans., 51 (2010); pp. 1051-1054.

[44] K. Edalati, Z. Horita, Mater. Sci. Eng. A, 528 (2011); pp. 7514-7523.

[45] S. Lee, Z. Horita, Mater. Trans., 53 (2012); pp. 38-45.

[46] M. Kawasaki, J. Mater. Sci., 49 (2014); pp. 18-34.

[47] A. Loucif, R.B. Figueiredo, T. Baudin, F. Brisset, T.G. Langdon, Mater. Sci. Eng. A, 527 (2010); pp. 4864-4869.

[48] H. Gleiter, Prog. Mater. Sci., 33 (1989); pp. 223-315.

[49] R. Birringer, Mater. Sci. Eng. A, 117 (1989); pp. 33-43.

[50] H. Gleiter, Nanostruct. Mater., 1 (1992); pp. 1-19.

[51] K. Lu, Mater. Sci. Eng. R, 16 (1996); pp. 161-221

[52] M. Furukawa, Z. Horita, M. Nemoto, R.Z. Valiev, T.G. Langdon, Phil. Mag. A, 78 (1998); pp. 203-216.

[53] F.A. Mohamed, Y. Li, Mater. Sci. Eng. A, 298 (2001); pp. 1-15.

[54] K.S. Kumar, H. Van Swygenhoven, S. Suresh, Acta Mater., 51 (2003); pp. 5743-5774.

[55] R.Z. Valiev, I. Sabirov, A.P. Zhilyaev, T.Z. Langdon, JOM 64 (2012); pp. 1134-1142.

[56] R.W. Armstrong, Mater. Trans., 55 (2014); pp. 2-12.

[57] R.Z. Valiev, Mater. Trans., 55 (2014); pp. 13-18.

[58] M.A. Meyers, A. Mishra, D.J. Benson, Prog. Mater. Sci., 51 (2006); pp. 427-556.

[59] S.A. Firstov, T.G. Rogul, O.A. Shut, Funct. Mater., 16 (2009); pp. 364-373.

[60] K.J. Kurzydłowski, B. Ralph, J. Bucki, A. Garbacz, Mater. Sci. Eng. A, 205 (1996); pp. 127-132.

Figure captions

Fig. 1 Thin disk processed by HPT showing cutting for the TEM samples (on left) and the three planes used for the TEM observations (on right).

Fig. 2 Bright field images in TEM (a-d) parallel to the axis of the HPT disk view with the corresponding SAED patterns, (e-h) cross-sectional plane parallel to the rotation direction and (i-l) cross-sectional plane perpendicular to the rotation direction: images of the alloy processed through (a,e,i) 1/2, (b,f,j) 1, (c,g,k) 5 and (d,h,l) 10 turns.

Fig. 3 Distribution of the number fractions of the misorientation angles of the grain boundaries of disks processed through 1/2, 1, 5 and 10 turns of HPT.

Fig. 4 Variation of hardness with distance from the centre of the disk for samples processed by HPT through different numbers of turns.

Fig. 5 Color-coded contour maps showing the Vickers microhardness across the surfaces of disks processed by HPT through different numbers of turns.

Fig. 6 Variation of hardness with equivalent strain for samples processed from 1/4 to 10 turns.

Fig. 7 The Hall-Petch relationship for coarse-grained samples and samples processed through various numbers of turns of HPT.

Table captions

Table 1 Average grain size of the 5483 aluminium alloy in a section parallel to the disk plane showing the initial state and after HPT.

Table 2 Grain width and grain elongation in the cross-sectional planes parallel (plane 2) and perpendicular (plane 3) to the rotation direction.

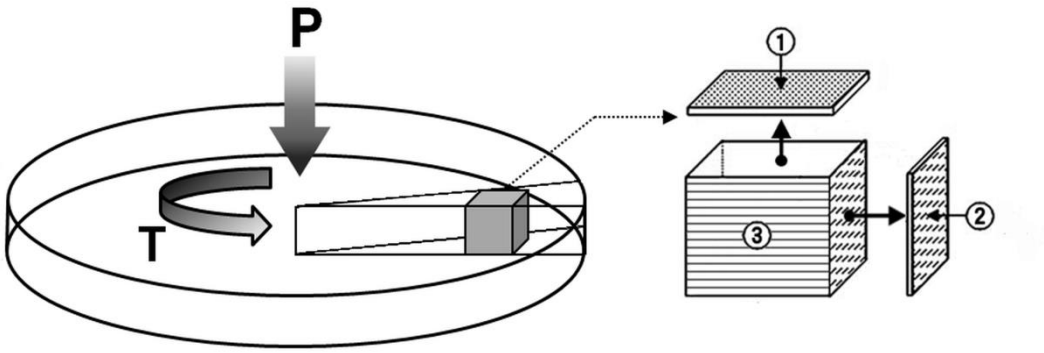

Fig. 1 Thin disk processed by HPT showing cutting for the TEM samples (on left) and the three planes used for the TEM observations (on right).

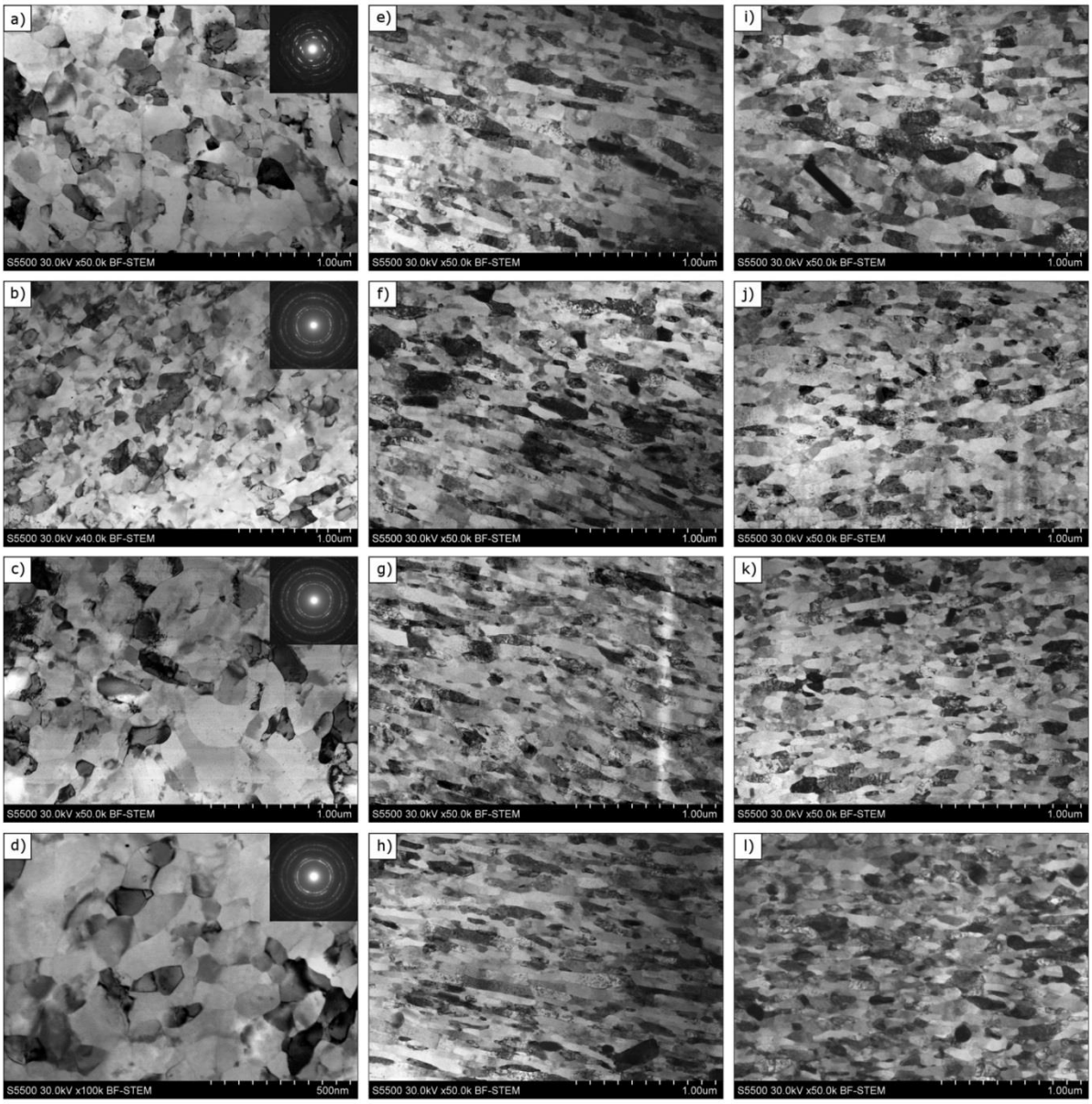

Fig. 2 Bright field images in TEM (a-d) parallel to the axis of the HPT disk view with the corresponding SAED patterns, (e-h) cross-sectional plane parallel to the rotation direction and (i-l) cross-sectional plane perpendicular to the rotation direction: images of the alloy processed through (a,e,i) 1/2, (b,f,j) 1, (c,g,k) 5 and (d,h,l) 10 turns.

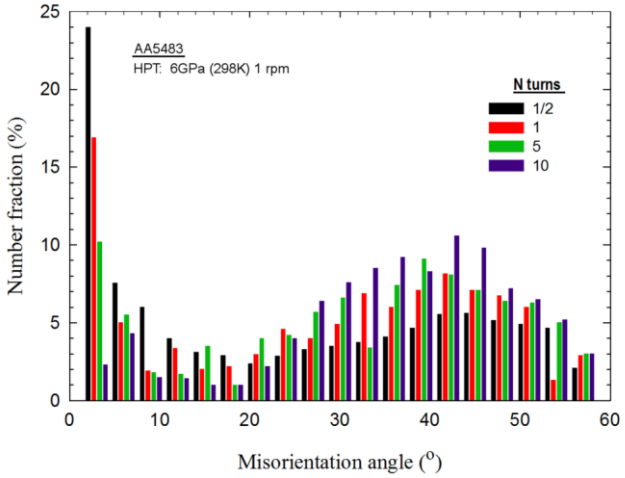

Fig. 3 Distribution of the number fractions of the misorientation angles of the grain boundaries of disks processed through 1/2, 1, 5 and 10 turns of HPT.

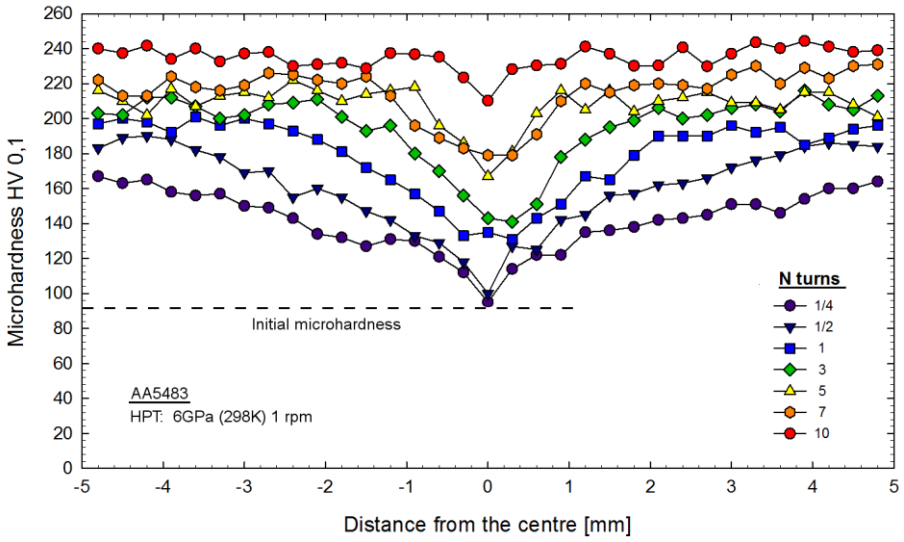

Fig. 4 Variation of hardness with distance from the centre of the disk for samples processed by HPT through different numbers of turns.

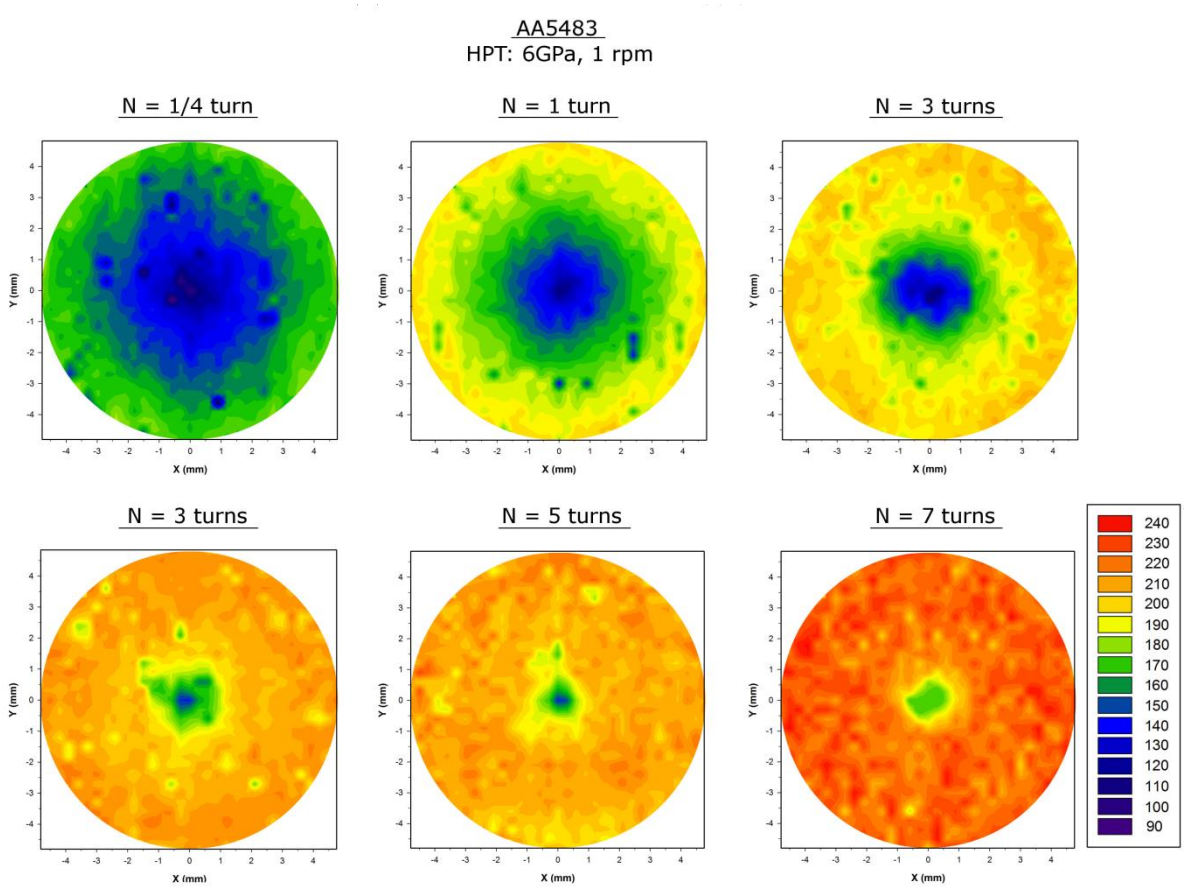

Fig. 5 Color-coded contour maps showing the Vickers microhardness across the surfaces of disks processed by HPT through different numbers of turns.

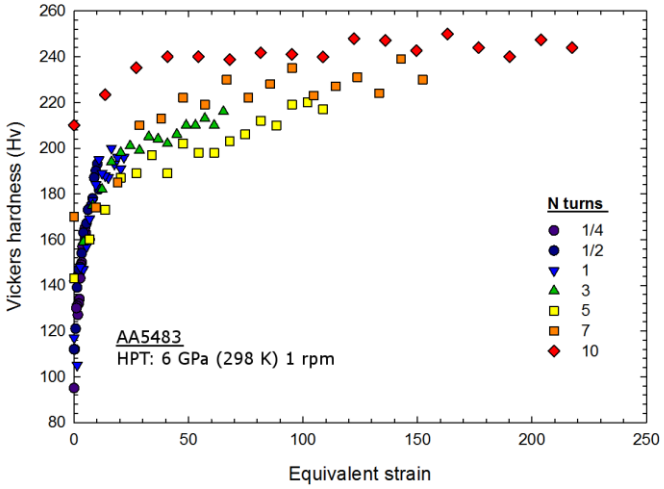

Fig. 6 Variation of hardness with equivalent strain for samples processed from 1/4 to 10 turns.

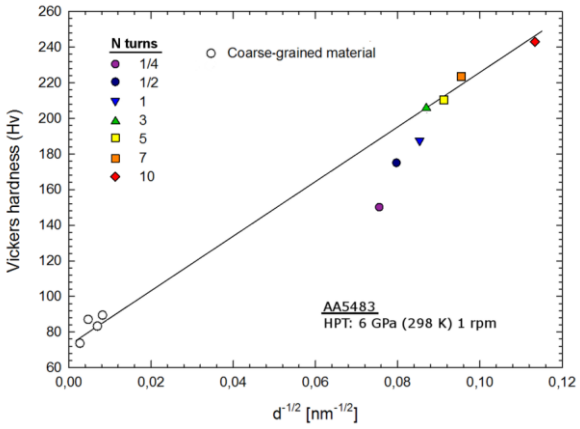

Fig. 7 The Hall-Petch relationship for coarse-grained samples and samples processed through various numbers of turns of HPT.

Table 1 Average grain size of the 5483 aluminium alloy in a section parallel to the disk plane showing the initial state and after HPT.

Number of turns	Initial state	1/4	1/2	1	3	5	7	10
Average grain size [nm]	25000	175	156	136	132	131	107	69
Standart deviation	10000	122	96	81	113	64	50	30

Table 2 Grain width and grain elongation in the cross-sectional planes parallel (plane 2) and perpendicular (plane 3) to the rotation direction.

Number of turns		1/2	1	5	10
Plane 2	Grain width [nm]	325	309	278	240
	Grain elongation factor	1.99	2.13	1.72	2.87
Plane 3	Grain width [nm]	173	159	148	140
	Grain elongation factor	1.51	2.08	2.23	2.05